Mansoura Engineering Journal

Volume 35 | Issue 3 Article 4

11-23-2020

Prediction of Surface Roughness of Turning Operations Using Computer Vision.

Elamir Gadelmawla
Associate Professor., Production Engineering and Mechanical Design Department., Faculty of Engineering., El-Mansoura University., 35516 Mansoura., Egypt., esamy@mans.edu.eg

Mansoura Engineering Journal, (MEJ), Vol. 35, No. 3, September 2010. M. 1

Prediction of Surface Roughness of Turning Operations Using Computer Vision

التنبؤ بخشونة الأسطح لعمليات الخراطة باستخدام الرؤية بالحاسب

E.S. Gadelmawla

Associate Professor, Prod. Eng. and Mech. Design Dept, Faculty of engineering, Mansoura University, Mansoura, Egypt

Email: esamy@mans.edu.eg

الملخص العربي:

من المعروف جيدا أن قياس خشونة الأسطح مهم جدا للتحكم في جودة الأجزاء المصنعة. وحديثا تم تطبيق نظم الرؤية بالحاسب في الصناعة للتحكم في الجودة والفحص المباشر. لذلك أصبح قياس خشونة الأسطح باستخدام الرؤية بالحاسب سهلا وممكنا. وتعتبر سمات بنية الصور من أهم الأساليب المطبقة في الصناعة في تطبيقات مختلفة. وفي هذا البحث تم استخدام سمات بنية الصور الخاصة بمعدل تكرار درجات الرمادي للتنبؤ بخشونة الأسطح للعينات المشغلة بواسطة عمليات الخراطة. وتم دراسة العلاقة بين سمات بنية الصور ومعاملات خشونة الأسطح لاكتشاف سمات بنية الصور التي لها علاقة قوية بمعاملات الخشونة، بحيث يمكن استخدامها للتنبؤ بخشونة الأسطح باستخدام الرؤية بالحاسب. وقد تم دراسة وشرح معامل الارتباط بين سمات بنية الصور ومعامل خشونة الأسطح المعروف (Ra). وقد تبين من البحث أن ست من سمات بنية الصور لها علاقة ارتباط قوية بمعامل الخشونة (Ra)، لذلك تم تطوير برنامج خاص يقوم بالتنبؤ بخشونة الأسطح للعينات المشغلة بالخراطة باستخدام هذه السمات. وقد أثبتت النتائج أن نسبة الخطأ بين قيم خشونة الأسطح المحسوبة بالبرنامج المقدم خلال هذا البحث وبين القيم الحقيقية لم تزد عن ±٧٪.

Abstract:

It is well known that measuring surface roughness is vital to quality control of the machined work piece. Recently, vision systems have been applied in industries for quality control and online inspection. Thus, measuring surface roughness using computer vision became easier and more flexible. Texture features are one of the most important techniques that have been utilized in industries in many applications. In this paper, the texture features of the gray level co-occurrence matrix (GLCM) have been utilized to predict surface roughness of specimens machined by turning operations. The relationship between GLCM texture features and surface roughness has been investigated to discover which texture features can be used to predict surface roughness. The correlation coefficient between each texture feature and the arithmetic average height (R_a) was calculated and discussed. The investigation showed that six texture features are highly correlated with R_a. Therefore, a software has been developed to predict surface roughness for specimens machined by turning operations using these texture features. The results showed that the maximum percentage of error between the actual R_a and the predicted R_a was about ±7%.

Keywords:

Surface roughness, Computer vision, Image processing, Texture Features.

Accepted September 30, 2010.

1. Introduction

The importance of control of surface roughness together with dimensional accuracy has been realized in the recent past. It is a generally accepted fact that surface finish greatly influences the functioning of machine parts. It also affects the resistance to wear, load carrying capacity, tool life, resistance to corrosion, fatigue resistance and ability to hold pressure and noise reduction in case of gears [1]. In the manufacturing industry, surfaces must be within certain limits of roughness. Therefore, measuring surface roughness is vital to quality control of the machining work piece.

The traditional method to measure surface roughness is stylus profiles. However, its contact nature makes the defect of scratching work pieces and the slow speed measurement unsuitable for online application [2, 3]. Therefore, non-contact methods like optical ways are used for the evaluation of surface finish. Machine vision is such an optical-based technique and its application in the field of inspection has been is increased [4]. In machine vision methods, surface roughness is measured according to the light scattered by specimens, which is recorded as an image by a CCD camera. The captured images are then analyzed according to their textures, which are described as a pattern with some kind of regularity.

Texture classification techniques are grouped up in five main groups in general, namely structural; statistical; signal processing; model-based stochastic; and morphology-based methods [5]. Out of the five groups, statistical and signal processing methods are the most widely used because they can be directly applied onto any type of texture. The rest are not as widely used because the structural methods need to implemented on structured textures which are naturally rare, the model based stochastic methods are not easily implemented due to the complexity to estimate the parameters and morphology-based methods are relatively new and the process are very simple, they may not promise very good textural features.

Statistical methods define textures as stochastic processes and characterize them by a few statistical features. Most relevant statistical approaches are Co-occurrence matrices [6], Markov random fields [7] and autocorrelation methods [8]. Signal theoretic approaches focus on periodic pattern resulting in peaks in the spatial frequency domain, e.g. Gabor filtering [9, 10] and wavelet decomposition [11].

Haralick texture features [6] based grey level co-occurrence matrix (GLCM) is one of the most widely used techniques for texture analysis. It captures second-order grey-level information, which is mostly related to human perception and the discrimination of textures. These texture features has proved its usefulness in a variety of image analysis applications, including textiles inspection [12, 13], food industries [14-16], biomedical [17, 18], remote sensing [19], quality control [20, 21] and industrial defect detection systems [22]. A detailed explanation of the GLCM and its calculation method is presented in [23].

The main drawback of the GLCM is that its computation is highly intensive especially for very large images, such as medical ones where the process requires a long computation time. Due to the importance of the grey level co-occurrence matrices (GLCM), researchers are still looking for efficient ways to compute the GLCM [24, 25].

Many researchers have tried to predict surface roughness using different methods. A review of the methods used to predict surface quality in machining process were introduced by Chen [26] and Benardos et al. [27]. In the field of the prediction of surface roughness using texture features, Zixin Chen et al. [28] introduced a machine vision method to assess surfaces roughness in different ambient light conditions using the gray-level co-occurrence matrix. They found that the ambient light affect the calculated roughness, therefore, they proposed a new multivariate-based method to minimize the effect of ambient light on roughness inspection. Xin and Wang [29] proposed a GLCM texture based fractal method to evaluate the surface roughness of fabric images by calculating two fractal parameters (box counting and the power spectrum) from the GLCM. They reported that the GLCM can represent a meaningful descriptive basis of fabric textures and the fractal parameters of the GLCM textures have the ability to evaluate the actual fabric surface roughness. Chuen-Lin Tien et al. [30] evaluated the surface roughness of titanium oxide films coated on glass substrates

by the GLCMs and entropy. They reported that the variation of entropy in titanium oxide films before and after film deposition was found to be related to the root-mean-square surface roughness. André et al. [31] calculated two GLCM parameters (correlation and entropy) from B-Mode images to assess non-invasive temperature estimation in a tissue mimic phantom and they reported that the Entropy values were capable of identifying variations of 2.0 °C and it was possible to quantify variations from normal human body temperature (37 °C) to critical values, as (41 °C).

The aim of this work is to investigate the relationship between GLCM texture features and surface roughness of surfaces machined by turning operations in order to discover the texture features that highly correlated with surface roughness. This can help to predict surface roughness using texture features.

2. Image Texture Features

Generally, the gray level co-occurrence matrix, $M_c(i,j)$ is calculated using the following equation:

$$M_c(i,j) = P(i,j) / \sum_{i,j}^{n} P(i,j) \quad (1)$$

Where $M_c(i,j)$ is defined as the co-occurrence of gray level occurring, $P(i,j)$ is the frequency of occurrence of gray levels i and j; and n refers to the total number of pixel pairs. A normalized matrix is produced by dividing each element of the GLCM by the summation of all elements.

In a previous work [32], all texture features that can be calculated from the GLCM (24 features) were collected from the literature and discussed. These texture features were used in this work to predict surface roughness. The mathematical equations of these texture features are listed next. If M_c is the normalized GLCM, i,j are the row and column of each element in the GLCM, and n is the number of the GLCM elements, then the following mathematical equations are used to calculate the GLCM texture features.

$$\text{ASM} = \sum_{i=0}^{n-1} \sum_{j=0}^{n-1} M_c(i,j)^2 \quad (2)$$

$$\text{CON} = \sum_{i=0}^{n-1} n^2 \sum_{j=0}^{n-1} M_c(i,j)\,(i-j)^2 \quad (3)$$

$$\text{COR} = \sum_{i=0}^{n-1} \sum_{j=0}^{n-1} \frac{M_c(i,j)\ ((i-\mu_x)(j-\mu_y))}{\sigma_x \sigma_y} \quad (4)$$

where μ_y is the mean for every column, σ_x is the Standard Deviation for every row and σ_y is the Standard Deviation for every column.

$$\text{CPR} = \sum_{i=0}^{n-1} \sum_{j=0}^{n-1} M_c(i,j)\ ((i+j)-(\mu_x+\mu_y))^4 \quad (5)$$

$$\text{CSH} = \sum_{i=0}^{n-1} \sum_{j=0}^{n-1} M_c(i,j)\ ((i+j)-(\mu_x+\mu_y))^3 \quad (6)$$

$$\text{CVAR} = \sigma / \mu \quad (7)$$

$$\text{DAVR} = \sum_{i=0}^{n-1} \text{i} * M_{c_{x-y}}(i) \quad (8)$$

Where: $M_{c_{x-y}}(k) = \sum_{i=0}^{n-1} \sum_{j=0}^{n-1} M_c(i,j)$ and $k = i - j$.

$$\text{DENT} = -\sum_{i=0}^{n-1} M_{c_{x-y}}(i) \ln\left(M_{c_{x-y}}(i)\right) \quad (9)$$

$$\text{DIS} = \sum_{i=0}^{n-1} \sum_{j=0}^{n-1} M_c(i,j)\,|i-j| \quad (10)$$

$$\text{DM} = \sum_{j=0}^{n-1} j \sum_{i=0}^{n-1} (0.5 M_c(i,j)|i-j|)^{0.5} \quad (11)$$

$$\text{DVAR} = \sum_{i=0}^{n-1} M_{c_{x-y}}(i)\,(i - DENT)^2 \quad (12)$$

$$\text{ENT} = -\sum_{i=0}^{n-1} \sum_{j=0}^{n-1} M_c(i,j) \ln(M_c(i,j)) \quad (13)$$

$$\text{IDM} = \sum_{i=0}^{n-1} \sum_{j=0}^{n-1} \frac{M_c(i,j)}{1+(i-j)^2} \quad (14)$$

$$\text{MaxP} = \max_{i,j}^{m,n} M_c(i,j) \quad (15)$$

$$\text{MCOR1} = \frac{ENT - HXY1}{Max(HX, HY)} \quad (16)$$

Where:

$$HXY1 = -\sum_{i=0}^{n-1} \sum_{j=0}^{n-1} M_c(i,j) \ln(M_{c_x}(i) M_{c_y}(j)),$$

$$M_{c_x}(i) = \sum_{j=0}^{n-1} M_c(i,j),$$

$$M_{cy}(j)=\sum_{i=0}^{n-1}M_c(i,j),$$

HX and HY are the entropies of $P_x(i)$ and $P_y(j)$, respectively.

$$\text{MCOR2}=\sqrt{1-\exp^{-2(HXY2-ENT)}} \quad (17)$$

Where:

$$HXY2=\sum_{i=0}^{n-1}\sum_{j=0}^{n-1}M_{cx}(i)M_{cy}(j)\ln(M_{cx}(i)M_{cy}(j))$$

$$\text{MEAN}(\mu)=\sum_{i=0}^{n-1}\sum_{j=0}^{n-1} i\,M_c(i,j) \quad (18)$$

$$\text{SAVR}=\sum_{i=2}^{2n} i\,M_{cx+y}(i) \quad (19)$$

Where: $M_{cx+y}(i+j)=\sum_{i=0}^{n-1}\sum_{j=0}^{n-1}M_c(i,j)$

$$\text{SDM}=\sum_{j=0}^{n-1} j\sum_{i=0}^{n-1}(0.5M_c(i,j)|i-j|) \quad (20)$$

$$\text{SENT}=-\sum_{i=2}^{2n}M_{cx+y}(i)\ln(M_{cx+y}(i)) \quad (21)$$

$$\text{SIM}=\sum_{i=0}^{n-1}\sum_{j=0}^{n-1}\frac{M_c(i,j)}{1+|i-j|} \quad (22)$$

$$\text{SVAR}=\sum_{i=2}^{2n}M_{cx+y}(i)\,(i-SENT)^2 \quad (23)$$

$$\text{VAR}=\sum_{i=0}^{n-1}\sum_{j=0}^{n-1}M_c(i,j)(i-\mu_x)^2 \quad (24)$$

Where: $\mu_x=\sum_{i=0}^{n-1} i\sum_{j=0}^{n-1}M_c(i,j)$

3. Experimental Work:

The vision system shown in Figure 1 has been employed to perform the experimental work in this research. The vision system consists of two main parts, hardware and software. The hardware was used to capture images for specimens machined by turning operations and the software was used to analyze the captured images.

The hardware consists of three main items: (1) IBM-compatible personal computer with Pentium IV processor and Windows operating system, (2) Incident light microscope to

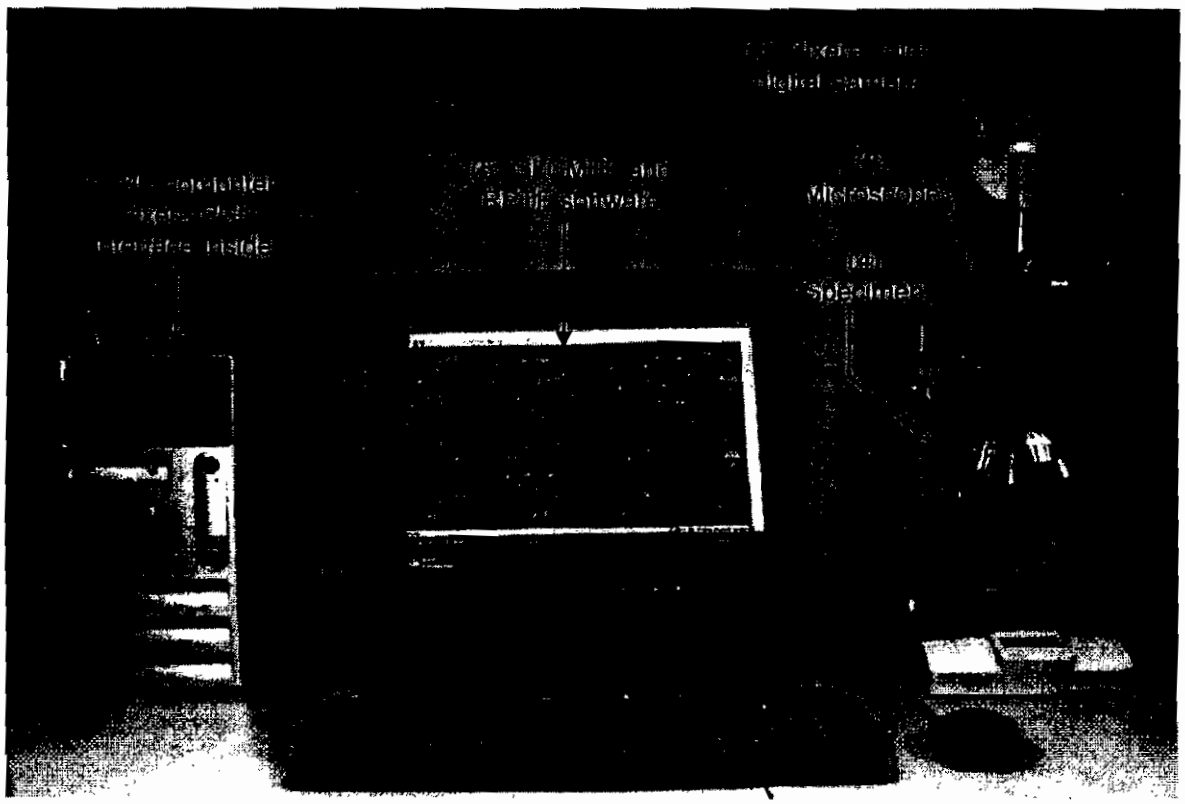

Fig. 1: Photograph of the employed vision system

magnify the surface to be analyzed and (3) a Pixera professional color digital camera system (1.2 million pixel) including Pixera PCI interface card with capturing software. The Pixera camera is fitted vertically on the microscope to capture an analogue image for surfaces to be analyzed. The Pixera PCI interface card is fitted inside the personal computer and it is used to digitize the analogue image into 1280x960 pixels with 16 bits of color.

The software, named GLCMTF (GLCM Texture Features), was fully developed in-house and was previously discussed in a previous work [33]. It is capable of calculating all GLCM texture features, discussed in section 2, for up to 100 position operators (direction θ and distance d) of the GLCM.

In this paper, a new module called RPTF (Roughness prediction from Texture Features) has been added to the GLCMTF software to predict roughness from texture features of captured images.

3.1 Specimens Preparation

A circular aluminum bar with 44 mm diameter was used, as a raw material, to produce 18 specimens with 15 mm height each. The surfaces of all specimens were machined using fine surface grinding to remove the effect of the previous machining. To produce surfaces with different roughness values, the specimens were divided into three groups (A, B, C) so that each group contains six specimens. A turning operation (face turning) was used to machine each group with different cutting conditions as shown in Table 1.

For each group, two cutting conditions were kept constant at intermediate values while the values of the other cutting condition were changed to a specific range of cutting condition. Cutting tools with tips of commercial type Widadur coated hard metal (TNMG160412P25), which has nose radius of 1.2 mm, were used to machine all specimens.

3.2 Roughness Measurements

Many parameters can be used to describe surface roughness. A detailed description of these parameters and its mathematical calculations are listed in a previous work [34]. The arithmetic average height (R_a), also known as center line average (CLA), is the most universally used roughness parameters for general quality control. Therefore, it will be used in this work as the roughness parameter to be correlated with texture features.

To measure the roughness of the machined specimens, a Handysurf E-10 [35] was used to measure the arithmetic average height (R_a) for all specimens. Each specimen was measured three times then the average of the three measurements was taken as the roughness value (R_a). Six specimens with different values of R_a (1.017, 2.148, 3.315, 4.265, 5.112, 6.782 μm) were selected from the machined specimens to produce a suitable range of roughness values. The selected specimens were used by the vision system, as discussed in the next section, to capture images for their machined surfaces in order to perform image analysis.

3.3 Capturing Images

The selected specimens were set under the microscope objective lens, then the vision system was used to capture three images for

Table 1: Cutting conditions used to produce different values of surface roughness (R_a)

Group	Constant cutting conditions	Changed cutting condition	Specimen No.					
			1	2	3	4	5	6
A	s =560, d_c = 0.25	f (mm/rev)	0.05	0.10	0.15	0.25	0.35	0.50
B	f=0.25, d_c = 0.15	s (rpm)	140	224	355	560	710	900
C	f=0.15, s = 560	d_c (mm)	0.10	0.15	0.25	0.7	0.50	1.0

each specimen at different areas. To avoid varying illumination conditions, which may affect the values of texture features, the microscope light was adjusted to constant light intensity while capturing all images. Figure 2 shows sample captured images for the selected specimens.

3.4 Image Analysis

To calculate the texture features for the selected six specimens, the following procedures were performed:

1- For each specimen, the three captured images were opened by the GLCMTF software, then the texture features were calculated for each image using a position operator of (1,90), i.e. (distance=1 and angle=90).

2- For each texture feature, the average of the values obtained from the three images was calculated and recorded as shown in Table 2.

3- The correlation coefficient between the values of each texture feature and the values of R_a was calculated using the following equation:

$$CC(a,b) = \frac{\sum(a-\bar{a})(b-\bar{b})}{\sqrt{\sum(a-\bar{a})^2 \sum(b-\bar{b})^2}} \qquad (25)$$

where CC is the correlation coefficient, a, b are the data sets of R_a and texture features, respectively, and $\bar{a}$, $\bar{b}$ are the averages of R_a and the texture features data sets, respectively. The calculated correlation coefficients are also shown in Table 2.

4- For the selected six specimens, the relationship between the values of R_a and the values of each texture feature was plotted to a graph using MS Excel for analysis.

5- Using MS Excel, the equation of correlation between R_a and each texture feature was obtained. These equations will be used later for the prediction process.

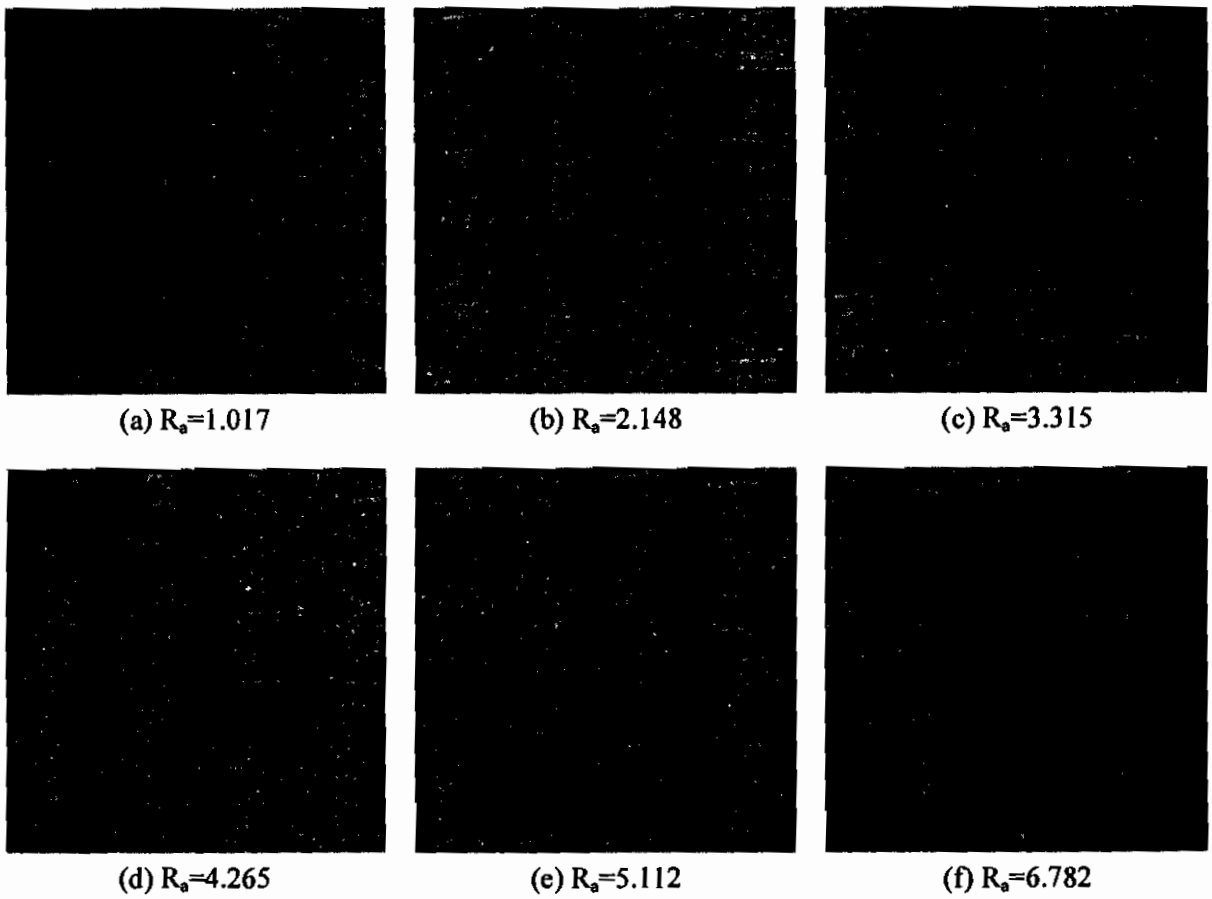

(a) R_a=1.017 (b) R_a=2.148 (c) R_a=3.315

(d) R_a=4.265 (e) R_a=5.112 (f) R_a=6.782

Fig. 2: Sample images of aluminum specimens machined with different cutting parameters (50X magnification)

Table 2: Calculated texture features (alphabetic sort) and their correlation coefficients with R_a

Texture Features	Value of R$_a$ (µm)						Correlation Coefficient (CC)
	2.01	2.48	3.46	4.26	5.42	6.49	
ASM	0.062617	0.062623	0.06262	0.062627	0.062633	0.062647	0.930
CON	123.80	131.70	137.30	122.57	117.37	99.33	0.745
COR	3.02E-04	3.05E-04	3.01E-04	3.08E-04	3.16E-04	3.10E-04	0.713
CPR	3.17E+08	3.10E+08	3.20E+08	3.13E+08	3.03E+08	3.17E+08	0.165
CSH	-626667	-471333	-491000	-429667	-360000	-340667	0.929
CVAR	0.66033	0.67333	0.67050	0.67333	0.67867	0.68067	0.891
DAVE	7.349	7.418	7.693	7.267	7.016	6.486	0.779
DENT	2.915	2.906	2.964	2.922	2.893	2.838	0.623
DgVAR	2.00E-06	2.00E-06	2.00E-06	2.00E-06	2.00E-06	2.00E-06	N/A
DIS	7.349	7.418	7.693	7.267	7.016	6.486	0.779
DM	176.80	181.88	188.13	179.58	176.20	166.93	0.584
DVAR	737000	712000	713500	703333	689000	688000	0.934
ENT	7.090	7.094	7.123	7.082	7.050	7.010	0.782
IDM	0.330333	0.336667	0.3315	0.335667	0.340333	0.346333	0.870
MaxP	0.250	0.250	0.250	0.250	0.250	0.250	N/A
MCOR1	0.31357	0.32297	0.31040	0.31967	0.32757	0.34023	0.793
MCOR2	0.962323	0.964803	0.962255	0.964977	0.967337	0.971170	0.875
MEAN	86.30	84.17	85.05	83.80	82.20	82.73	0.860
SAVR	17849.0	17051.0	17185.5	16818.7	16371.7	16382.7	0.917
SDM	3.675	3.709	3.8465	3.633	3.507667	3.243	0.779
SENT	866.3	851.0	852.5	845.7	837.0	836.0	0.935
SIM	0.39167	0.39733	0.39100	0.39633	0.40200	0.40900	0.845
SVAR	490899	476184	475692	469769	461942	459429	0.953
VAR	3249	3213	3250	3186	3110	3172	0.712

4. Results and Discussions

In this section, the correlations between R_a and all texture features has been investigated. In addition, the process of predicting R_a from the captured images using the texture features has been discussed.

4.1 Correlations between R_a and the Image Texture Features

Figure 3 shows the correlation coefficients between all texture features and the value of R_a. The texture features are sorted according to their correlation coefficients (from the highest to lowest). The following points could be observed from Figure 3:

1- Six texture features (SVAR, SENT, DVAR, ASM, CSH, SAVR) are highly correlated with R_a (correlation coefficient greater than or equal to 0.9). Therefore, these texture features will be used later, in this paper, to predict the surface roughness from captured images. Figure 4 shows the relationship between these texture features and R_a. The equation of correlation between each texture feature and R_a is also shown in the graph.

2- Five texture features (CVAR, MCOR2, IDM, MEAN, SIM) are relatively highly correlated with R_a (correlation coefficient ranges between 0.8 and 0.9). Figure 5 shows the relationship between two of these texture features (CVAR and MCOR2) and R_a.

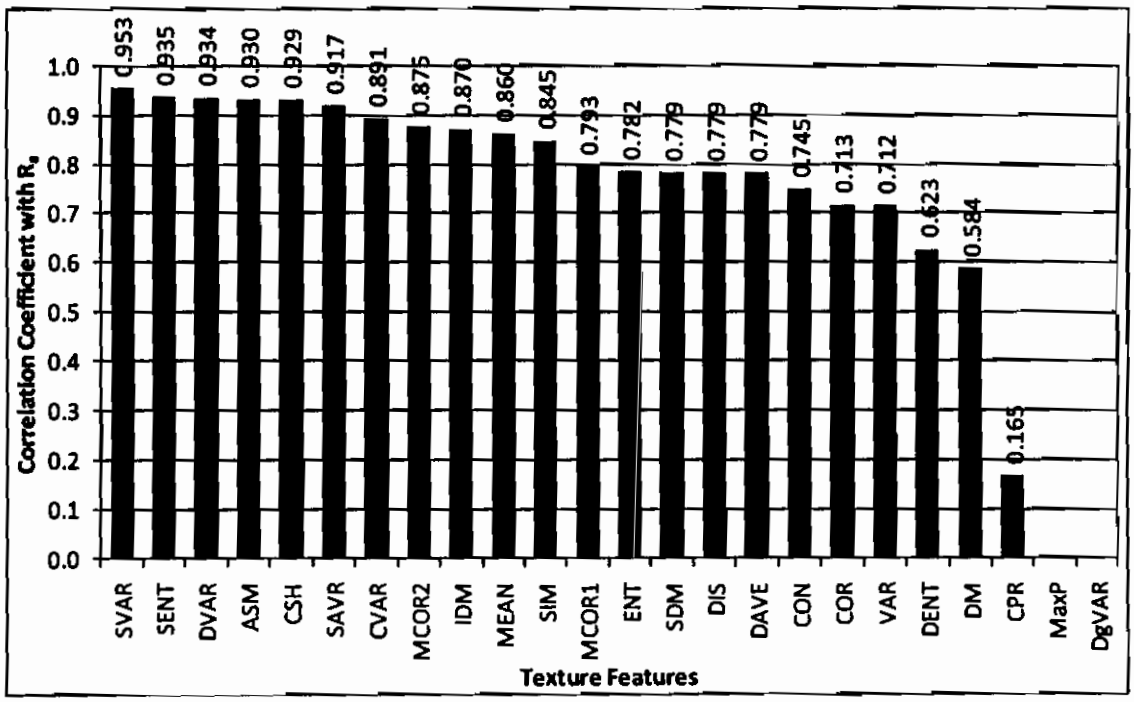

Fig. 3 Texture features sorted according to their correlation coefficients with R_a

3- Other texture features (ENT, SDM, DIS, DAVE, CON, COR, VAR, DENT, DM, CPR) do not have good correlation with R_a (correlation coefficient less than 0.80). Figure 6 shows the relationship between the two texture features that have lowest correlation (DM and CPR) and R_a.

4- No correlation could be obtained for both MaxP and DgVAR texture features. Figure 7 shows the graphs of these texture features.

4.2 Roughness Prediction:

The equations of correlation of the highly correlated texture features were obtained from the graphs plotted by Excel, then the value of R_a was calculated from these equations. Regarding to the equations shown in Figure 4, y represents the texture feature and x represents R_a, hence, the value of R_a can be predicted from these texture features using the following equations:

$$R_a = (492112 - SVAR)/5245.6 \quad (26)$$

$$R_a = (867.26 - SENT)/5.0823 \quad (27)$$

$$R_a = (738127 - DVAR)/8212.6 \quad (28)$$

$$R_a = (ASM - 6.261E^{02})/4.898E^{06} \quad (29)$$

$$R_a = (CSH + 628405)/46429 \quad (30)$$

$$R_a = (17871 - SAVR)/245.91 \quad (31)$$

To predict the values of R_a from the captured images, a new module called RPTF (roughness prediction from texture features), Fig. 8, has been added to the GLCMTF software to perform the prediction process. Equations 26-31 have been entered to the RPTF module in order to calculate R_a from the calculated texture features.

To verify the introduced system, the RPTF module was used to predict the value of *Ra* for three specimens selected from the samples produced during this work. The values of R_a for the three samples were calculated as the average of three measurements for each specimen and they were 2.867, 3.243, and 5.451. Table 3 shows the calculated texture features, the predicted values of R_a, and the percentage of error between the actual R_a (measured R_a) and the predicted R_a. The percentage of error was calculated as follows:

$$\text{Error (\%)} = 100\times(\text{Actual } R_a - \text{Predicted } R_a) / \text{Actual } R_a \quad (32)$$

From table 3, it can be seen that the maximum percentage of error between the actual R_a and the predicted R_a is about ±7%.

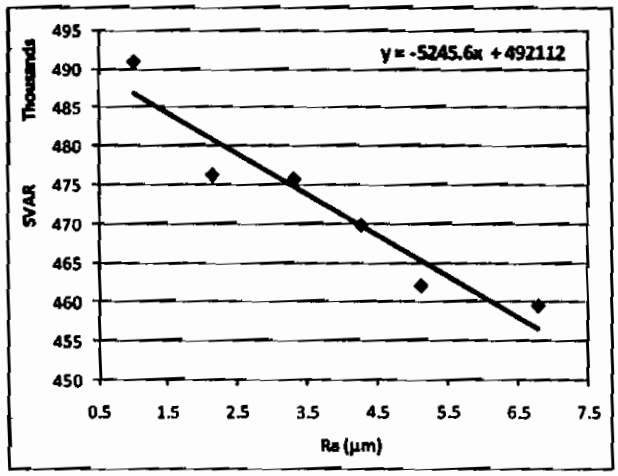

(a) SVAR (Correlation Coefficient =0.953)

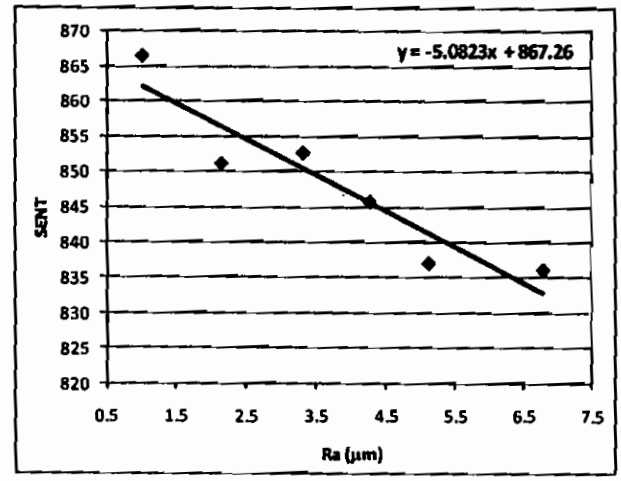

(b) SENT (Correlation Coefficient =0.935)

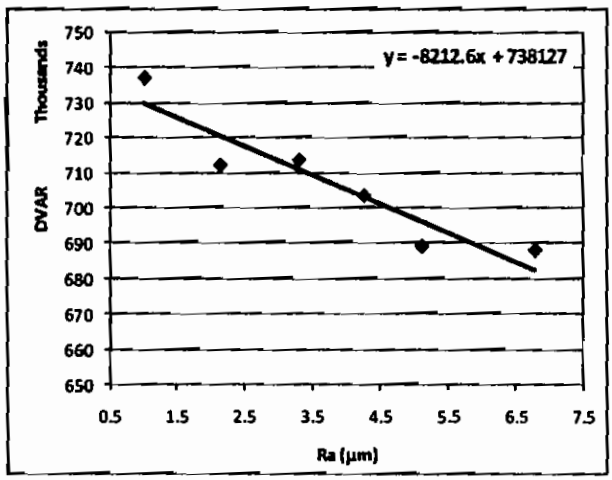

(c) DVAR (Correlation Coefficient =0.934)

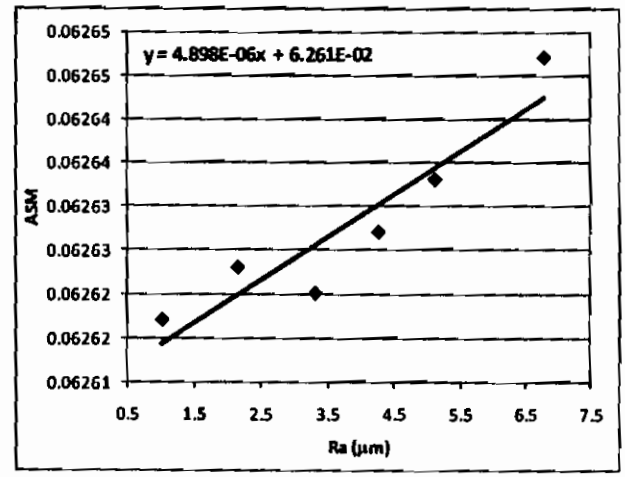

(d) ASM (Correlation Coefficient =0.930)

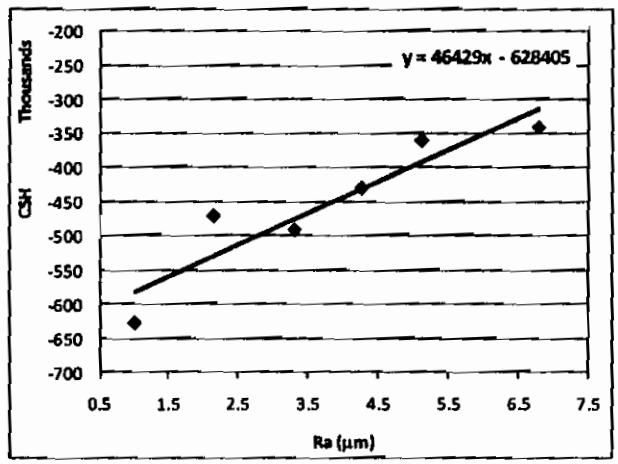

(e) CSH (Correlation Coefficient =0.929)

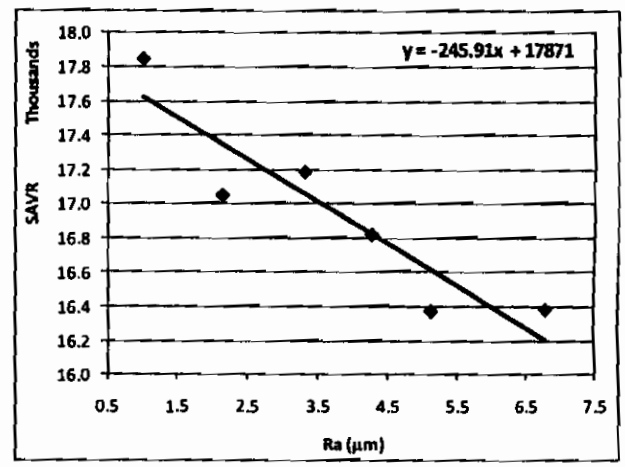

(f) SAVR (Correlation Coefficient =0.917)

Fig. 4 Relationship between highly correlated texture features and R_a (correlation coefficient >= 0.90)

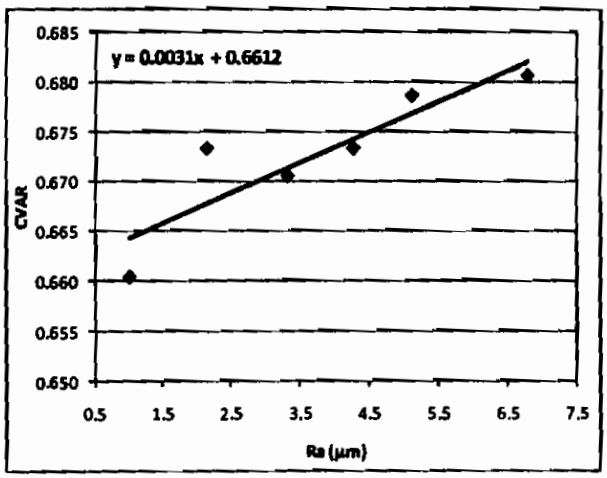

(a) CVAR (Correlation Coefficient =0.891)

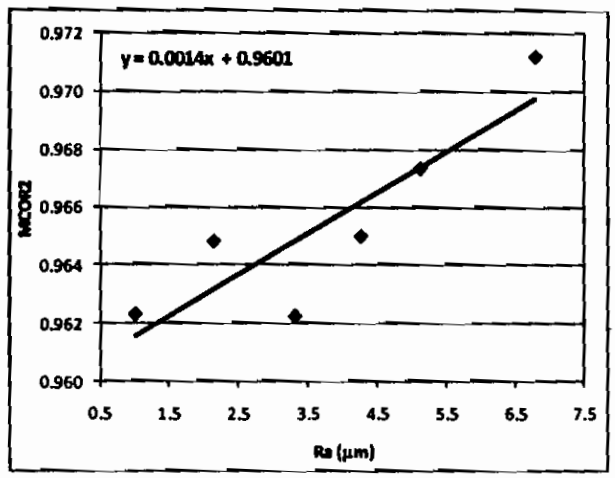

(b) MCOR2 (Correlation Coefficient =0.875)

Fig. 5 Relationship between some texture features of relatively high correlation and R_a (correlation coefficient ranges between 0.80 and 0.90)

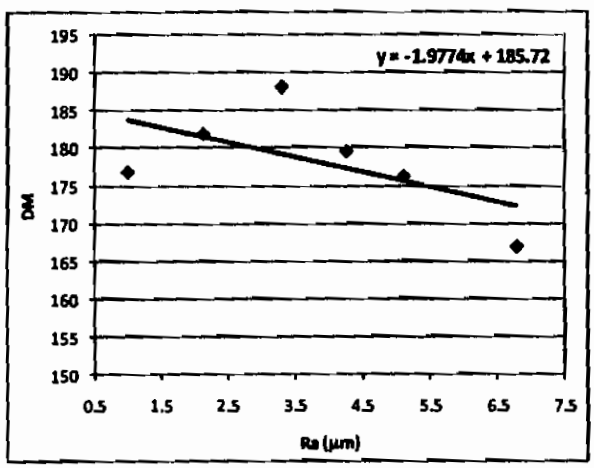

(a) DM (Correlation Coefficient =0.584)

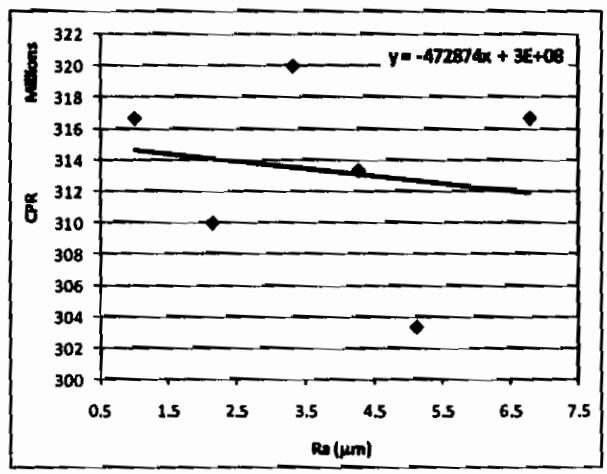

(b) CPR (Correlation Coefficient =0.165)

Fig. 6 Relationship between some texture features of lowest correlation and R_a (correlation coefficient less than 0.80)

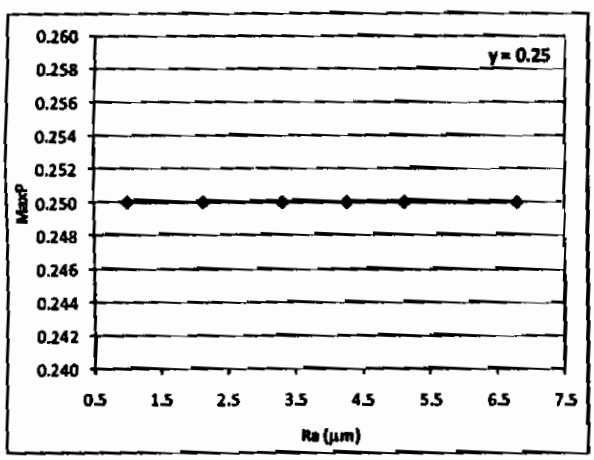

(a) MaxP Correlation Coefficient =N/A

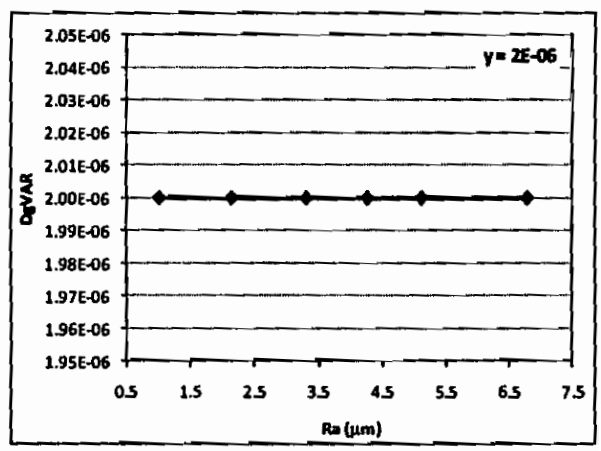

(b) DgVAR Correlation Coefficient =N/A

Fig. 7 texture features that have no correlation with the roughness parameters Ra

Table 3: Comparison between the actual and predicted roughness values for three selected samples

SVAR	477959.4	2.698	5.89	475876.9	3.095	4.56	464173.9	5.326	2.29
SENT	853.1	2.786	2.83	851.3	3.131	3.45	840.4	5.278	3.17
DVAR	713628.8	2.983	-4.05	709834.6	3.445	-6.23	690370.7	5.815	-6.68
ASM	0.062624	2.783	2.93	0.062626	3.354	-3.42	0.062636	5.315	2.49
CSH	-487539.4	3.034	-5.82	-472171.4	3.365	-3.76	-383956.3	5.265	3.41
SAVR	17210.7	2.685	6.35	17111.6	3.088	4.78	16435.6	5.837	-7.08

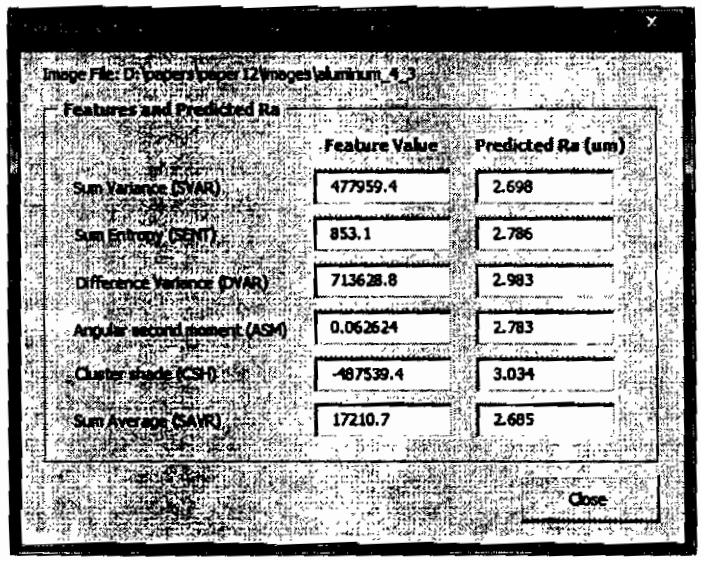

Fig. 8 predicted roughness (R_a) from the calculated texture features for sample 1

Conclusions:

An investigation of the relationship between GLCM texture features and surface roughness of specimens machined by turning operations has been done. It was found that six texture features (SVAR, SENT, DVAR, ASM, CSH, SAVR) are highly correlated with Ra (correlation coefficient greater than or equal to 0.9). The equations of correlation of these texture features were obtained from the graphs plotted by Excel, then prediction equations were derived to calculate the value of R_a from the calculated value of texture feature. The six texture features have been successfully employed to predict surface roughness of similar specimens with known values of R_a. The prediction results showed that the maximum percentage of error between the actual R_a and the predicted R_a was about ±7%.

References:

1- Singh S.K., Srinivasan K. and Chakraborty D., Acoustic characterization and prediction of surface roughness, J. Mater. Process. Technology, 2004, 152, 127–130.

2- Chen J.C. and Savage M., A Fuzzy-Net-Based Multilevel In-Process Surface Roughness Recognition System in Milling Operations, Int J Adv Manuf Technology, 2001, 17, 670–676.

3- Lu R.S., Tian G.Y., and Gledhill D., Grinding surface roughness measurement based on the co-occurrence matrix of speckle pattern texture, Applied Optics, 2006, 45 (35), 1–9.

4- Elango V., and Karunamoorthy L., Effect of lighting conditions in the study of surface roughness by machine vision-an experimental design approach, Int J Adv

Manuf Technology, 2008, 37 (1-2), 92–103.

5- Chen Y.Q., Novel Techniques for Image Texture Classification., PhD thesis, University of Southampton, United Kingdom, 1995.

6- Haralick R.M., Shanmugam K., and Dinstein I., Textural features for image classification. IEEE Transactions on Systems Man and Cybernetics, 1973, 3, 610–621.

7- Lei Wang and Jun Liu, Texture classification using multi-resolution markov random field models, Pattern Recognition Lett., 1999, 20 (2), 171–182.

8- PietikSainen M., Ojala T., and Xu Z., Rotation-invariant texture classification using feature distributions, Pattern Recognition, 2000, 33, 43–52.

9- Jain A.K., and Farrokhnia F., Un-supervised texture segmentation using Gabor, lters, Pattern Recognition, 1991, 24 (12), 1167–1186.

10- Randen T. and HusHy J.H., Multichannel filtering for image texture segmentation, Opt. Eng., 1994, 33 (8), 2617–2625.

11- Jing-Wein Wang, Chin-Hsing Chen, Wei-Ming Chien, and Chih-Ming Tsai, Texture classification using non-separable two-dimensional wavelets, Pattern Recognition Lett., 1998, 19(13), 1225–1234.

12- Abouelela A., Abbas H.M., Eldeeb H., Wahdan A.A. and Nassar S.M., Automated vision system for localizing structural defects in textile fabrics, Pattern Recognition Letters, 2005, 26 (10), 1435-1443.

13- Carfagni M., Furferi R. and Governi L., A real-time machine-vision system for monitoring the textile raising process, Computers in Industry, 2005, 56(8-9), 831-842.

14- Chandraratne M.R., Samarasinghe S., Kulasiri D. and Bickerstaffe R., Prediction of lamb tenderness using image surface texture features, Journal of Food Engineering, 2005, 28, 1-8.

15- Paliwal J., Visen N.S., Jayas D.S. and White N.D.G., Cereal grain and dockage identification using machine vision, Biosystems Engineering, 2003, 85, 51–57.

16- Thybo A.K., Szczypiński P.M., Karlsson A.H., Dønstrup S., Stødkilde-Jørgensen H.S. and Andersen H.J., Prediction of sensory texture quality attributes of cooked potatoes by NMR imaging (MRI) of raw potatoes in combination with different image analysis methods. Journal of Food Engineering, 2004, 61, 91–100.

17- Karkanis S.A., Iakovidis D.K., Maroulis D.E., Karras D.A., and Tzivras M., Computer aided tumor detection in endoscopic video using color wavelet features, IEEE Trans. Inf. Technol. Biomed., 2003, 7, 141–152.

18- Tahir M.A., Bouridane A. and Kurugollu F., An FPGA based coprocessor for GLCM and haralick texture features and their application in prostate cancer classification, Analog Integr. Circ. Signal Process, 2005, 43, 205–215.

19- Baraldi A. and Parmiggiani F., An investigation of the textural characteristics associated with gray level co-occurrence matrix statistical parameters, IEEE Trans. Geosci. Remote Sens., 1995, 33 (2), 293-304.

20- Torabi, M., Ardekani, R.D., and Fatemizadeh, E., Discrimination between alzheimerapos disease and control group in MR-image based on texture analysis using artificial neural network, International Conference on Biomedical and Pharmaceutical Engineering, 2006, 11–14, 79–83.

21- Mayumi D., Sabino U., Costa L.F., Rizatti E.G., and Zago M.A., A texture approach to leukocyte recognition, Special Issue on Imaging in Bioformatics Part III, Real-Time Imaging, 2008, 10, Academic Press, 205–216.

22- Iivarinen J., Heikkinen K., Rauhamaa J., Vuorimaa P., and Visa A., A defect detection scheme for web surface inspection, Int. J. Pattern Recogn. Artif. Intell., 2000, 735–755.

23- Gadelmawla E.S., A vision system for surface roughness characterization using the gray level co-occurrence Matrix, NDT&E International, 2004, 37, 577–588.

24- Iakovidis D.K., Maroulis D.D., and Bariamis D.G., FPGA architecture for fast parallel computation of co-occurrence matrices, Microprocessors and Microsystems, 2007, 31, 160–165.

25- Siéler L., Tanougast C., and Bouridane A., A scalable and embedded FPGA architecture for efficient computation of

grey level co-occurrence matrices and Haralick textures features, Microprocessors and Microsystems, 2010, 34, 14–24

26- Chen Lu, Study on prediction of surface quality in machining process, journal of materials processing technology, 2008, 205, 439–450.

27- Benardos P.G. and Vosniakos G.C., Predicting surface roughness in machining: a review, International Journal of Machine Tools & Manufacture, 2003, 43, 833–844

28- Zixin Chen, Zhisheng Zhang, Jinfei Shi, Ruwen Chen, Ren Huang, and Chaofeng Zhang, A multivariate method for surface roughness vision inspection in different ambient light. Proceedings of 2008 IEEE International Conference on Mechatronics and Automation (ICMA 2008), 324-328, 5-8 Aug. 2008.

29- Xin N.D. and Wang Georganas, GLCM texture based fractal method for evaluating fabric surface roughness, Canadian Conference on Electrical and Computer Engineering, CCECE '09, 104 – 107, 3-6 May 2009, John's, NL.

30- Chuen-Lin Tien, You-Ru Lyu, and Shiao-Shan Jyu, Surface flatness of optical thin films evaluated by gray level co-occurrence matrix and entropy, Applied Surface Science, 2008, 254, 4762–4767.

31- André V. Alvarenga, César A. Teixeira, Maria Graça Ruano, and Wagner C.A. Pereira, Influence of temperature variations on the entropy and correlation of the Grey-Level Co-occurrence Matrix from B-Modc images, Ultrasonics, 2010, 50, 290–293.

32- Gadelmawla E.S., Eladawi A.E., Abouelatta O.B. and Elewa I.M., Investigation of the cutting conditions in milling operations using image texture features, Journal of Engineering Manufacture, Part B, 2008, 222(11), 1395-1404.

33- Gadelmawla E.S., Eladawi A.E., Abouelatta O.B. and Elewa I.M, Application of Computer Vision for the Prediction of Cutting Conditions in Turning Operations, Journal of Engineering Manufacture, Part B, 2009, 223 (7), 791-800.

34- Gadelmawla E.S., Koura M.M., Maksoud, T.M.A. Elewa, I.M. and Soliman H.H., Roughness parameters. Journal of Materials Processing Technology, 2002, 123 (1), 133-145.

35- Handysurf E-10, "Advanced Metrology Systems Limited", 2 Pomeroy Drive, OADBY Industrial Estate, OADBY Leicester, LE2 5NE, England.

Abbreviations

ASM	Angular Second Moment
CCD	Charge Coupled Device
CON	Contrast
COR	Correlation
CPR	Cluster Prominence
CSH	Cluster Shade
CVAR	Coefficient Of Variation
DAVR	Difference Average
DENT	Difference Entropy
DIS	Dissimilarity
DM	Diagonal Moment
DVAR	Difference Variance
ENT	Entropy
GLCM	Gray Level Co-Occurrence Matrix
GLCMTF	GLCM Texture Features
IDM	Inverse Difference Moment
MaxP	Maximum Probability
MCOR1	Mean Correlation 1
MCOR2	Mean Correlation 2
MEAN	Mean
RPTF	Roughness Prediction from Texture Features
SAVR	Sum Average
SDM	Second Diagonal Moment
SENT	Sum Entropy
SIM	Similarity
SVAR	Sum Variance
VAR	Variance

Nomenclature

dc	Depth of cut (mm)
f	Feed (mm/rev)
M_c	Matrix of the gray level co-occurrence
s	Speed (rpm)
R_a	Arithmetic average height